The Effect of CO Adsorption at Room Temperature on the Structure of Supported Pt Particles

Barbara L. Mojet,*,† Jeffrey T. Miller,‡ and Diederik C. Koningsberger†

Debye Institute, Department of Inorganic Chemistry, Utrecht University, P.O. Box 80083, 3508 TB Utrecht, The Netherlands, and Amoco Research Center, E-1F, 150 West Warrenville Road, Naperville, Illinois 60563

Received: August 5, 1998; In Final Form: December 31, 1998

To improve the understanding of the applicability of CO−FTIR spectroscopy for probing the electronic properties of catalysts, the effect of CO adsorption on the geometry of small metal particles in Pt/LTL and Pt/SiO_2 catalysts with varying support acidities was determined by comparison of X-ray absorption spectra before and after CO adsorption. At room temperature, the platinum particles (first shell coordination number $N > 5$) supported on SiO_2 were stable under CO atmosphere. By contrast, the smaller platinum particles ($N < 5$) in zeolite LTL reconstructed with the formation of very small platinum−CO aggregates upon admission of CO at room temperature. For both Pt/SiO_2 and Pt/LTL the linear-to-bridge ratio (L/B) of the CO infrared bands is a function of the support acidity/alkalinity. In the case of Pt/SiO_2, the L/B ratio directly reflects the electronic properties of the catalytically active metal, since the metal particles do not reconstruct. The results show that the structure of the platinum particles in LTL zeolite, which participate in catalytic reactions is not the same as the Pt−CO aggregate analyzed by FTIR. Nevertheless, both the catalytic activity and L/B ratio are a function of support acidity.

Introduction

Infrared spectroscopy of adsorbed CO is an established technique to characterize supported metal particles.[1−7] Several factors affect the FTIR spectra, like particle size, surface coverage, and ion−dipole interactions. For example, the CO absorption band was suggested to consist of separate contributions of CO adsorbed on sites with different metal−metal coordination numbers.[1] Since the surface of a metal particle consists of atoms with different coordination numbers due to their location at edges, corners, or faces,[2] the metal particle size determines the final shape of the CO absorption band. Also, ion−dipole interactions between adsorbed CO and cations in zeolite lattices were shown to introduce a fine structure in the spectra.[3] Third, the frequency of the absorption band increases with higher surface coverage due to dipole−dipole interactions between adjacent CO molecules.[4] The integrated intensity ratio of linear/bridge (L/B) bound CO was found to depend on the electron density of a metal surface by both experimental[5,6] as well as theoretical studies.[7] The higher the electron density of the metal, the lower the L/B ratio. This phenomenon was used to determine the influence of support acidity/alkalinity on the electron density of supported metal particles.[5,6]

Despite the general application of FTIR of adsorbed CO for characterization of supported metal catalysts, interpretation of the infrared data is still a matter of debate. Recently, Stakheev and co-workers presented an infrared study on Pt/K-LTL as a function of CO partial pressure.[8] In that study, they suggested that CO induces the formation of new, neutral platinum−carbonyl clusters inside the zeolite. While anionic platinum clusters can be synthesized from precursor complexes as $[Pt(NH_3)_4]^{2+}$ and CO,[9−12] these complexes have not been prepared from reduced platinum metal particles. EXAFS and FTIR studies have shown the reconstruction of reduced rhodium particles supported on Al_2O_3 or TiO_2 after admission of CO,[13,14] resulting in monorhodium−carbonyl clusters. In addition, a metal particle size effect for rhodium was shown. Rhodium particles with an average first shell coordination number $N \sim 7$ did not reconstruct under CO atmosphere while very small metal particles ($N \sim 4$) formed Rh geminal carbonyl complexes.[15]

Shifts in the frequency and changes in the linear-to-bridged ratio are often used to probe indirectly the metal electron density near the Fermi-level in order to correlate electronic structure with observed catalytic activity. For example, for platinum and palladium catalysts the turnover frequency for neopentane hydrogenolysis decreases with increasing support alkalinity.[5,6] In addition, the integrated intensity ratio linear to bridged bound CO decreased in the same order.[5,6,16] Furthermore, for Pt/SiO_2 there was a linear correlation of the linear/bridged ratio with catalytic activity.[6] For Pt/LTL catalysts the correlation was nonlinear.

To better understand the applicability of linear-to-bridged ratio of adsorbed CO for probing the electronic properties of catalysts, the effect of CO adsorption on the geometry of small metal particles in Pt/LTL and Pt/SiO_2 with varying support acidities has been determined by XAFS spectroscopy. X-ray absorption data show that the larger platinum particles supported on SiO_2 are stable, while the smaller platinum particles on zeolite LTL reconstruct upon exposure to CO at room temperature. It is proposed that platinum−CO aggregates are formed in LTL zeolite. The different behavior toward CO for Pt/SiO_2 and Pt/LTL is most likely due to the larger metal particles on SiO_2. The applicability of CO-FTIR spectroscopy for probing electronic properties of catalysts is also discussed.

* Corresponding author. Present address: Schuit Institute for Catalysis, Eindhoven University of Technology, P.O. Box 513, 5600 MB Eindhoven, The Netherlands.

† Utrecht University.

‡ Amoco Research Center.

10.1021/jp983283e CCC: $18.00
Published on Web 03/23/1999

TABLE 1: Elemental Analysis and Platinum Dispersion

catalyst	wt. % K	wt. % Al	wt. % Pt	H/Pt
Pt/LTL(0.63)	8.3	9.5	1.0	0.53
Pt/LTL(0.96)	11.8	8.5	1.0	0.89
Pt/LTL(1.25)	15.9	8.8	1.0	0.88
Pt/SiO_2-Al(0.10)		0.10	1.54	0.60
Pt/SiO_2			1.40	0.58
Pt/SiO_2-K(1.14)	1.14		1.48	1.35

Experimental Section

Catalyst Preparation. The acidity of the LTL zeolite support was varied by either impregnating a commercial K-LTL zeolite with KNO_3 or exchanging with NH_4NO_3 to give K/Al ratios ranging from 0.63 to 1.25. Each LTL zeolite was calcined at 225 °C and analyzed for potassium and aluminum. Platinum was added by incipient wetness impregnation with $[Pt(NH_3)_4](NO_3)_2$ followed by drying at 120 °C. The catalysts are designated Pt/LTL(*x*) with (*x*) representing the K/Al molar ratio.

The silica supports were prepared by ion exchange of SiO_2 (15 g in 500 mL of H_2O at 60 °C) with increasing amounts of KOH followed by calcination at 400 °C. Also, an acidic silica was prepared by ion exchange of SiO_2 with excess of $Al(NO_3)_3$ followed by washing, drying, and calcination at 400 °C. Platinum was added by incipient wetness impregnation with $[Pt(NH_3)_4](NO_3)_2$ followed by calcination at 225 °C. The catalysts are designated Pt/SiO_2-*X* with *X* representing the wt % Al or K.

Metal dispersion was determined by H_2 chemisorption after reduction at 300 °C according to the double isotherm method. The dispersion (H/Pt) and the elemental analysis of all catalysts are reported in Table 1.

Fourier Transform Infrared Spectroscopy. The transmission infrared spectra were recorded on a Perkin-Elmer 1720-X Fourier transform spectrometer at a spectral resolution of 4 cm^{-1}. The catalysts were pressed in thin self-supporting wafers and placed in an in-situ transmission infrared cell. The catalyst was reduced in H_2 at 300 °C and cooled to room temperature. Subsequently, the sample was purged with He for 10 min followed by flowing 20% CO in He gas for 10 min, after which the CO absorbance spectrum was collected. The samples are denoted by Pt/LTL-[CO] or Pt/SiO_2-[CO]. For the Pt/LTL catalysts a gas flow with a small amount of water was used to prevent ion−dipole interactions between K^+ and absorbed CO.[3] Spectra were corrected for the absorption of the support and gas-phase CO.

X-ray Absorption Fine Structure (XAFS) Experiments. The samples were characterized by XAFS spectroscopy at the SRS Daresbury (U.K.) at Wiggler station 9.2, using a Si(220) double crystal monochromator. The measurements were done in transmission mode using ion chambers filled with Ar to have a μx of 20% in the first and a μx of 80% in the second ion chamber. The monochromator was detuned to 50% maximum intensity at 12 250 eV to avoid higher harmonics present in the X-ray beam.

Each sample was pressed into a self-supporting wafer (calculated to have an absorbance of 2.5) and placed in an in-situ cell.[17] It was dried at 120 °C and subsequently reduced at 300 °C (heating rate 5 °C/min) for 1 h in flowing hydrogen (purified and dried). Subsequently, the sample was cooled under flowing H_2 and spectra were taken at liquid nitrogen temperature (Pt/LTL or Pt/SiO_2-*X*). The sample was allowed to warm to room temperature and exposed to a CO/He (1/1) gas flow (purified and dried) for 15 min at room temperature. XAFS spectra were taken subsequently at liquid nitrogen temperature (Pt/LTL-[CO] or Pt/SiO_2-[CO]).

XAFS Data Analysis. Data analysis was performed by multiple shell fitting in *R*-space.[18] Different backscatterers were identified by applying the difference file technique[19] using phase-corrected Fourier transforms.[20] The difference file technique is based on the fact that a single scattering contribution in a model spectrum correctly describing the experimental data must be equal to the experimental spectrum minus all other model contributions:

$$\chi_i = \chi_{\text{experiment}} - \sum_{j=1,j\neq i}^{n} \chi_j \qquad \text{with} \qquad \chi_{\text{model}} = \sum_{j=1}^{n} \chi_j$$

Data for the phase shifts and backscattering amplitudes were obtained from reference compounds. Pt foil was used as a reference for Pt−Pt contributions; $Na_2Pt(OH)_6$ was used for Pt−O contributions.[21] To analyze adsorbed CO, Pt−C and multiple scattering Pt−O* references are necessary. XAFS data of crystalline $Ir(CO)_{12}$ were used to extract Ir−C and multiple scattering Ir−O* backscattering amplitudes and phase shifts.[22] Since phase shift and backscattering amplitude are transferable between Pt and Ir, these data could be used to calculate a model spectrum for Pt−C and Pt−O* contributions.[22]

The variances in imaginary and absolute parts were used to determine the fit quality, according to

$$k^n \text{ variance} = 100\frac{\int[k^n(\text{FT}_{\text{model}}(R) - \text{FT}_{\text{experiment}}(R))]^2}{\int[k^n\,\text{FT}_{\text{experiment}}(R)]^2}$$

Models with variances in absolute and imaginary parts below 1% are considered to represent very good models for the experimental data. The errors in the fit parameters are estimated to be 5% in coordination number (*N*), 1% in distance (*R*), 5% in Debye−Waller factor ($\Delta\sigma^2$), and 10% in inner potential correction (ΔE_0).

Results

EXAFS: Structure of Pt/LTL and Pt/SiO_2 after Reduction. Parts a−f of Figure 1 show the Fourier transforms of the XAFS data of Pt/LTL and Pt/SiO_2 with varying support acidities. The dotted lines indicated the best fit obtained after *R*-space analysis; the parameters are given in Tables 2 and 3. It can be seen that the metal particles in the Pt/LTL series are very small with average Pt−Pt coordination numbers less than 4.5. The long Pt−O distance of approximately 2.68 Å is in accordance with previous studies on Pt/LTL.[23] No potassium could be detected near the platinum particles.

The Pt/SiO_2 series shows larger platinum particles with Pt−Pt coordination numbers between 5.3 and 7.6. Each catalyst also exhibited an oxygen contribution at around 2.2 Å. No potassium or aluminum could be detected near the platinum particles.

FTIR: Adsorption of CO on Pt/LTL and Pt/SiO_2. The transmission infrared spectra of Pt/LTL and Pt/SiO_2 are shown in Figure 2a,b, respectively. Two regions of adsorbed CO can be assigned: at higher wavenumbers absorption due to linearly coordinated CO and at lower wavenumbers a band caused by CO in bridged coordination to the metal atoms. For Pt/LTL and Pt/SiO_2 the linear- as well as the bridged-coordinated CO absorption bands shifted to lower wavenumbers as the support alkalinity increased. The shifts are more pronounced for the Pt/LTL series than for the Pt/SiO_2 series. The line shapes for Pt/SiO_2-Al(0.10) and Pt/SiO_2 were sharper than that of Pt/SiO_2-K(1.14) consistent with the different Pt particle sizes of the catalysts.[1,2] Larger metal particles result in sharper absorption

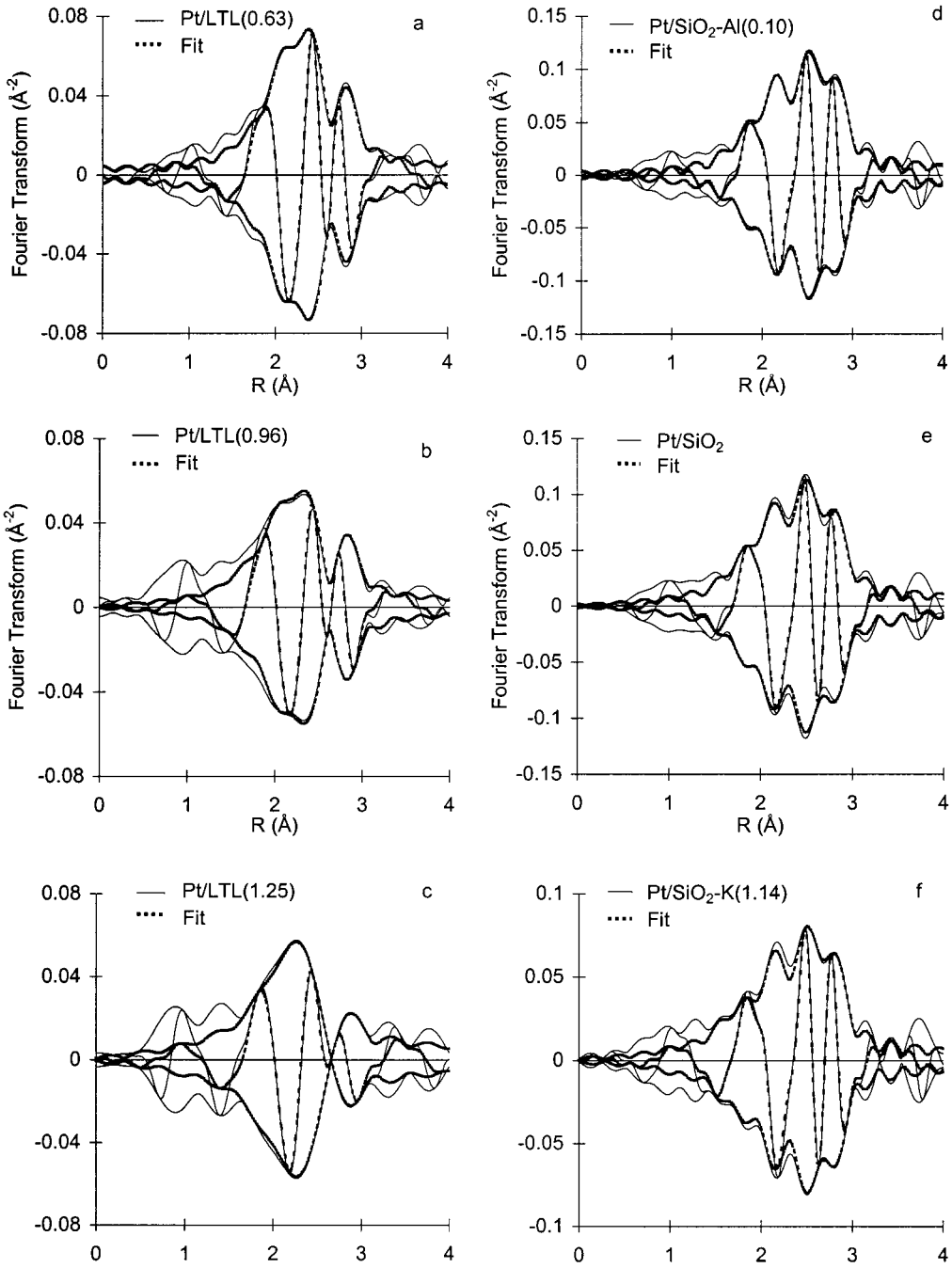

Figure 1. k^1-weigthed Fourier transforms of experimental data (solid line) and calculated model spectra (dotted line): (a) Pt/LTL(0.63), Δk = 3.2−14.0 Å^{-1}; (b) Pt/LTL(0.96), Δk = 3.2−14.0 Å^{-1}; (c) Pt/LTL(1.25), Δk = 3.2−11.0 Å^{-1}; (d) Pt/SiO_2-Al(0.10), Δk = 3.2−14.8 Å^{-1}; (e) Pt/SiO_2, Δk = 3.2−14.8 Å^{-1}; (f) Pt/SiO_2-K(1.14), Δk = 3.2−14.8 Å^{-1}.

TABLE 2: Fit Parameters (Δk = 3.2−14.0 Å^{-1}, ΔR = 1.60−3.20 (Å) and Variances for Model Spectra Pt/LTL

						k^1-variance (%)	
catalyst	scatterer	N (±5%)	R (Å, ±1%)	$\Delta\sigma^2$ (±5%) (10^{-3} Å^2)	ΔE_0 (eV) (±10%)	im part	abs part
Pt/LTL(0.63)	Pt	3.7	2.74	4.6	−2.2	0.7	0.4
	O	2.1	2.69	4.8	7.3		
Pt/LTL(0.96)	Pt	4.5	2.74	3.5	−1.5	0.6	0.4
	O	1.6	2.68	0.9	4.5		
Pt/LTL(1.25)[a]	Pt	2.3	2.72	3.3	9.3	0.3	0.1
	O	3.0	2.64	10.5	5.6		

[a] k = 3.2−11.0 Å^{-1}, due to lower signal-to-noise ratio, as only one spectrum was available for this catalyst.

bands, with their maximum positioned at higher wavenumbers. The bigger platinum particles of Pt/SiO_2-Al(0.10) and Pt/SiO_2 are thus reflected in the CO absorption line shape. However, there is no relation between Pt particle size and the integrated intensity ratio linear/bridged (L/B) CO (Table 4). The small shoulder visible at 1940 cm^{-1} in the FTIR spectrum of Pt/LTL-

TABLE 3: Fit Parameters (Δk = 3.2−14.8 Å^{-1}, ΔR = 1.60−3.10 Å) and Variances for Model Spectra Pt/SiO_2

						k^1-variance (%)	
catalyst	scatterer	N (±5%)	R (Å) (±1%)	$\Delta\sigma^2$ (10^{-3} Å^2) (±5%)	ΔE_0 (eV) (±10%)	im part	abs part
Pt/SiO_2-Al(0.10)	Pt	7.4	2.77	2.2	0.4	0.5	0.1
	O	0.5	2.23	3.0	−15.6		
Pt/SiO_2	Pt	7.7	2.77	2.6	2.1	0.7	0.3
	O	0.5	2.21	1.2	−16.4		
Pt/SiO_2-K(1.14)	Pt	5.3	2.77	2.3	1.2	0.6	0.4
	O	0.5	2.12	3.5	−9.3		

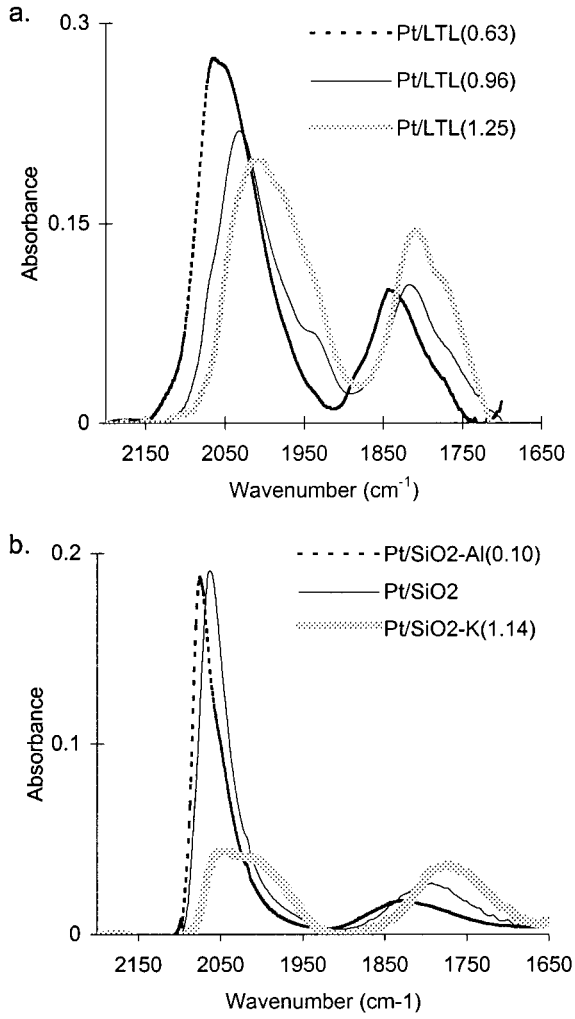

Figure 2. (a) Transmission FTIR spectra of CO adsorbed on Pt/LTL catalysts. (b) Transmission FTIR spectra of CO adsorbed on Pt/SiO_2 catalysts.

TABLE 4: Integrated Intensity Ratio Linear/Bridged Bound CO on Pt/LTL and Pt/SiO_2

catalyst	linear/bridged ratio	catalyst	linear/bridged ratio
Pt/LTL(0.63)	3.2	Pt/SiO_2-Al(0.10)	3.8
Pt/LTL(0.96)	2.3	Pt/SiO_2	3.1
Pt/LTL(1.25)	1.7	Pt/SiO_2-K(1.14)	1.1

(0.96) is often observed in the IR spectra of Pt/LTL samples and has been assigned to ion−dipole interactions between K^+ and adsorbed CO.[3] The integrated intensity ratio of linear/bridged CO decreases with increasing support alkalinity for Pt/LTL as well as Pt/SiO_2. In other words, CO prefers bridged to linear coordination with higher support alkalinity.

EXAFS: Influence of CO Adsorption on the Structure of Pt/LTL(0.96). Figure 3 shows the experimental data and Fourier transforms of Pt/LTL(0.96) after reduction and exposure

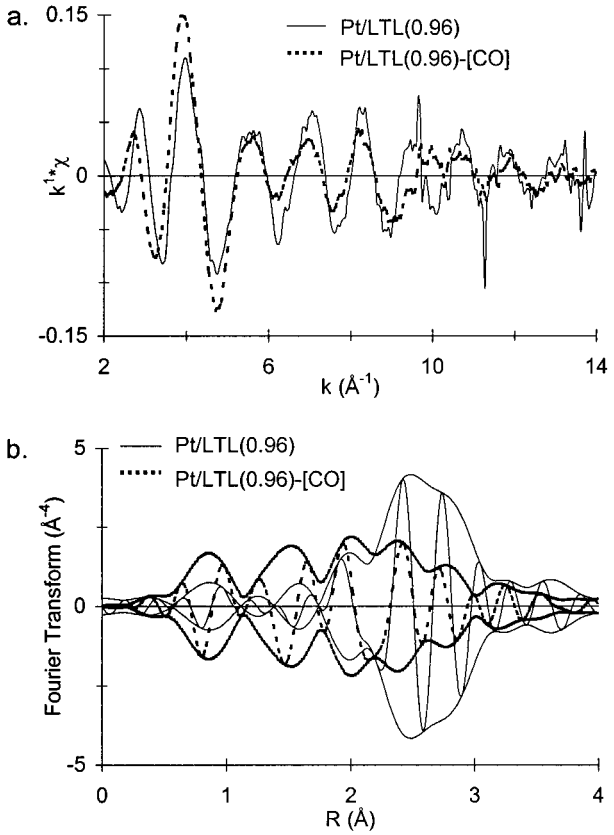

Figure 3. (a) k^1-weighted experimental data of Pt/LTL(0.96) (solid line) and Pt/LTL(0.96)-[CO] (dotted line), (b) Fourier transform (k^3, Δk = 3.2−12.7 Å^{-1}) of spectra in (a).

to CO (Pt/LTL(0.96)-[CO]). Comparison of the spectra reveals major differences in both the imaginary and absolute parts. Between 0.5 and 2.0 Å, the amplitude of the absolute part for Pt/LTL(0.96)-[CO] is greater, while in the region from 2.0 to 3.0 Å the amplitude is lower compared to Pt/LTL(0.96). Also between 0.5 and 2.0 Å, the nodes in the imaginary part of the Fourier transform are shifted, indicating that the structure of the platinum particles has been altered.

Comparison of the k^3 Pt−Pt phase-corrected Fourier transforms of Pt/LTL(0.96) and Pt/LTL(0.96)-[CO] taken over 6.0−12.7 Å^{-1}, which is dominated by Pt−Pt scattering (Figure 4a), clearly shows that the average first shell Pt−Pt coordination number has decreased upon CO adsorption. To determine the Pt−Pt coordination parameters, the spectrum was first analyzed in R-space (ΔR: 2.3−3.0 Å) with a k^3-weighted Fourier transform taken over this limited range in k-space (6.0−12.7 Å^{-1}). Subsequently, the other scatterers were identified and all model parameters were optimized together. The model Pt−Pt EXAFS contribution obtained after full optimization is shown in Figure 4b together with the total spectrum of Pt/LTL(0.96)-[CO]. Thus, the Pt−Pt contribution indeed dominates the k^3-weighted Fourier transform taken from 6 to 12.7 Å^{-1}.

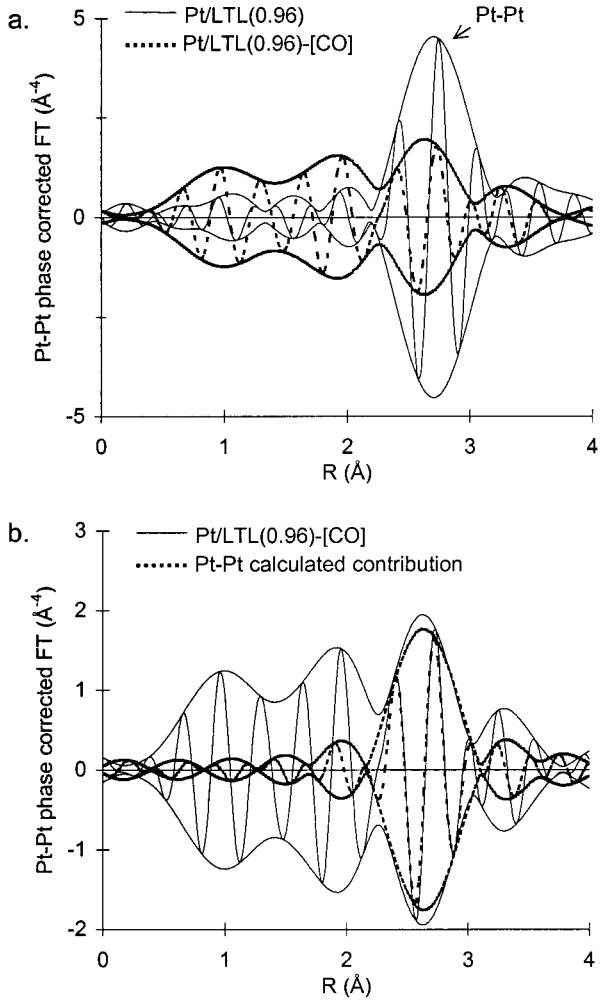

Figure 4. k^3-weighted, Pt−Pt phase corrected Fourier transform (Δk = 6.0−12.7 Å^{-1}) of (a) Pt/LTL(0.96) (solid line) and Pt/LTL(0.96)-[CO] (dotted line) and (b) Pt/LTL(0.96)-[CO] (solid line) and calculated Pt−Pt contribution (Table 5).

Figure 5 shows the experimental data and Fourier transform of Pt/LTL(0.96)-[CO] together with the model spectrum obtained after analysis in *R*-space (Table 5). Fitting of the spectra in *R*-space (k^1 and k^3 weighted, using different *k*-ranges) reveals Pt−Pt, Pt−C, Pt−O*, and Pt−O contributions. The resemblance of the experimental data and calculated spectrum in *k*- and *R*-space (Figure 5a,b) indicates that no additional backscatterers are present. The statistical significance of each contribution was over 85%.

Parts c−f of Figure 5 show the individual model contributions χ_i to the residual spectrum ($\chi_{\text{experiment}} - \sum_{j=1,j\neq i}^{n} \chi_j$). Both the imaginary and absolute parts of the Fourier transforms of the individual components and the residual spectra are in good agreement for all backscatterers. The EXAFS data analysis for Pt/LTL(0.96)-[CO] show that the Pt−Pt distance has contracted to 2.67 Å, together with a decrease of Pt−Pt coordination number from 4.2 to 2.2 after exposure of Pt/LTL(0.96) to CO at room temperature. In addition to these changes in the Pt coordination parameters, Pt−Pt scattering and Pt−C, Pt−O, and Pt−O* scattering were also detected.

EXAFS: Influence of Support Acidity/Alkalinity on Structure of Pt/LTL Catalysts after CO Adsorption. The Fourier transforms of the experimental data for all Pt/LTL and Pt/LTL-[CO] samples are shown in Figure 6. It can be seen that for all samples the EXAFS spectrum significantly changed after exposure to CO at room temperature. To check the influence of CO exposure on the Pt−Pt coordination, the k^3-weighted Fourier transforms for Δk (6.0−12.7 Å^{-1}) were compared (Figure 7). For Pt/LTL(0.63)-[CO] and Pt/LTL(1.25)-[CO], a decrease in amplitude between 2 and 3 Å is visible, similar to that for Pt/LTL(0.96)-[CO], showing that the Pt−Pt coordination has changed. Closer examination of the figure also reveals that the three Pt/LTL-[CO] spectra are clearly different from each other in shape and amplitudes, indicating that the final structure of the platinum particles with CO is different for each catalyst.

EXAFS: Effect of CO Adsorption on the Structure of Pt/SiO_2 Catalysts. Parts a−c of Figure 8 show k^1-weighted Fourier transforms of the experimental data for reduced Pt/SiO_2 together with Pt/SiO_2-[CO]. For each sample, there are small deviations after exposure to CO. However, shape and position of the imaginary parts do not change upon exposure to CO, indicating that the average local structure of platinum is essentially the same. To evaluate the Pt−Pt contribution, Pt−Pt phase corrected k^3-weighted Fourier transforms are compared for *k*: 6.0−12.7 Å^{-1} (Figure 8 d−f). The position and shape of the platinum EXAFS signal does not change upon CO exposure; however, the intensity slightly decreased for Pt/SiO_2-Al(0.10)-[CO] and Pt/SiO_2-[CO], while it increased for Pt/SiO_2-K(1.14)-[CO]. These changes in intensity can be attributed to differences in coordination number and/or disorder in the Pt−Pt contribution. The *R*-space model fits (ΔR: 1.0−3.5, optimized in both k^1- and k^3) of the spectra of Pt/SiO_2-[CO] are reported in Tables 6−8. The Fourier transforms of the model spectra and the experimental data are shown in Figure 9. The spectra agree very well for *R*: 1.2−3.3 Å. The Pt−Pt coordination numbers are similar or slightly smaller than those of the reduced catalysts, and moreover, the Pt−Pt distances are identical for the samples with and without CO. In addition to Pt−Pt coordination, also Pt−C and Pt−O* could be detected, originating from adsorbed CO.

Discussion

Structure of Catalysts after Reduction. All catalysts contained metallic platinum particles, as can be concluded from the observed Pt−Pt distances that are similar to the Pt−Pt distance in Pt-foil (2.77 Å). The Pt/LTL samples consist of metal particles with the average first shell coordination number smaller than 4.5. Assuming closest packing of Pt atoms, the average metal particle in Pt/LTL contains approximately 4−6 atoms. These small particles easily fit inside the pockets of a zeolite LTL channel. The Pt/SiO_2 catalysts have larger first shell coordination numbers ($N > 5$), and consequently contain more Pt atoms per particle. Assuming a spherical closest packing, the particle sizes range approximately from 15 to 50 atoms, going from Pt/SiO_2-K(1.14) to Pt/SiO_2-Al(0.10). The very small platinum particles in zeolite LTL are believed to be stabilized by the zeolite geometrical pore structure, which is absent on the SiO_2 surface.

In addition, a scattering contribution from the support oxygen atoms could be observed. The long Pt−O distance of approximately 2.7 Å for the Pt/LTL samples is in accordance with previous studies on Pt/LTL and is attributed to the presence of interfacial hydrogen after low-temperature reduction.[24] The short Pt−O distance of 2.2 Å for the Pt/SiO_2 catalysts indicates that the Pt particles are in direct contact with the support oxygen atoms, despite the low (300 °C) reduction temperature. The coordination distance is similar to those in Ir/Al_2O_3[22] and Pt/Al_2O_3[25] catalysts after high-temperature reduction (>450 °C).

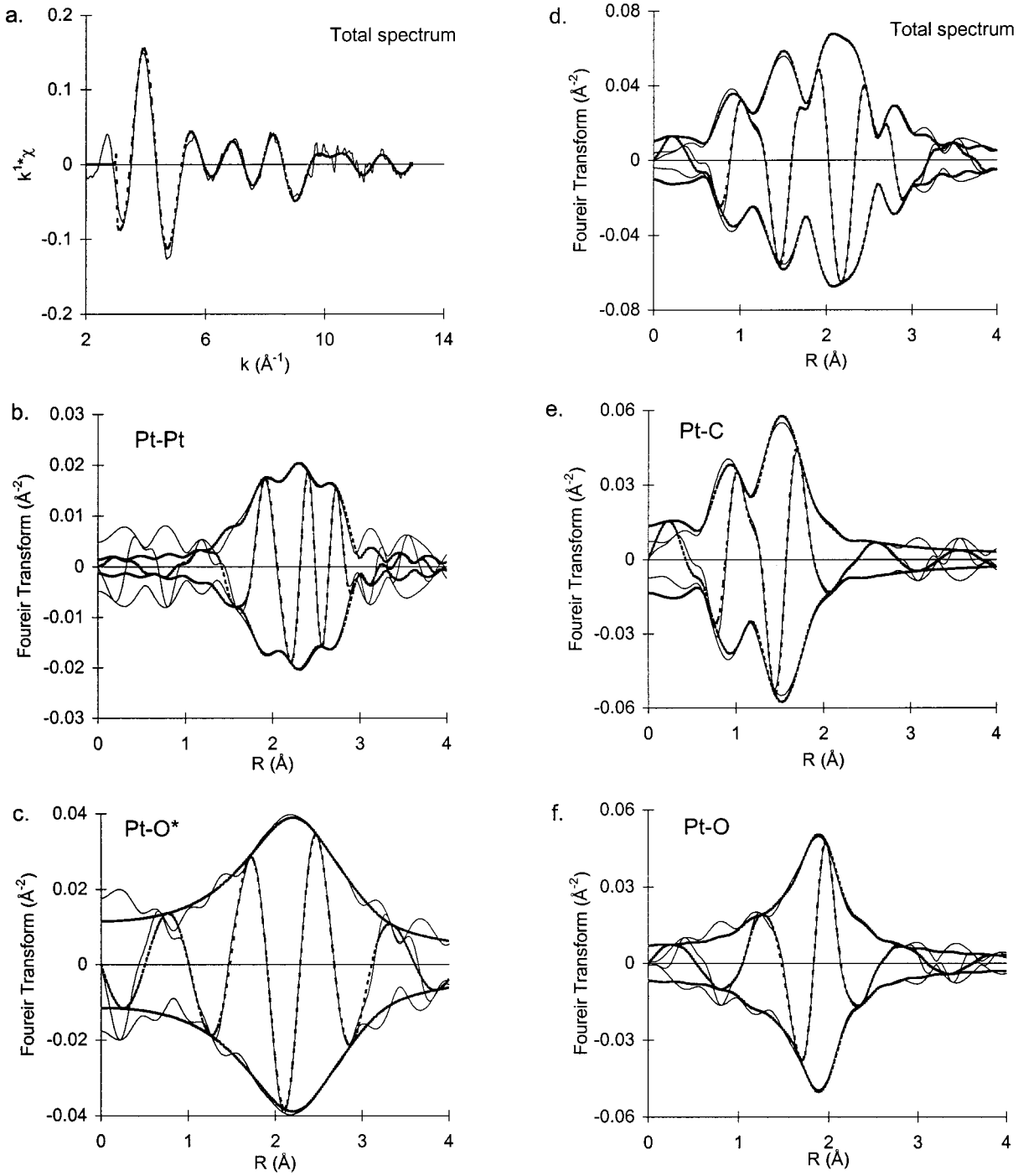

Figure 5. (a) Experimental EXAFS data of Pt/LTL(0.96)-[CO] (solid line) and calculated spectrum with parameters given in Table 6 (dashed line). (b) Fourier transform [k^1, $\Delta k = 3.2-12.7$ Å^{-1}] of EXAFS data of Pt/LTL(0.96)-[CO] (solid line) and calculated spectrum with parameters given in Table 6 (dashed line). (c) Pt−Pt: calculated contribution (dotted line) and EXAFS data minus calculated [(Pt−C) + (Pt−O*) + (Pt−O)] (solid line). (d) Pt−C: calculated contribution (dotted line) and EXAFS data minus calculated [(Pt−Pt) + (Pt−O*) + (Pt−O)] (solid line). (e) Pt−O*: calculated contribution (dotted line) and EXAFS data minus calculated [(Pt−Pt) + (Pt−C) + (Pt−O)] (solid line). (f) Pt−O: calculated contribution (dotted line) and EXAFS data minus calculated [(Pt−Pt) + (Pt−C) + (Pt−O*)] (solid line).

The difference in metal−support characteristics between the zeolite and SiO_2 supported catalysts can be due to (i) the larger metal particles for Pt/SiO_2 and (ii) the differences in support properties.

Influence of CO Adsorption on Particle Structure of Pt/LTL. Analysis of Pt/LTL(0.96)-[CO] revealed a contraction of the Pt−Pt distance from 2.74 to 2.67 Å, accompanied by a decrease in Pt−Pt coordination number from 4.5 to 2.2. Both features indicate a reconstruction of the metallic platinum particles (±6 atoms) into smaller aggregates (±3 Pt atoms). The

TABLE 5: Structural Parameters for Pt/LTL(0.96)-[CO], *R*-Space Fit, $\Delta k = 3.2-12.7$ Å^{-1}, $\Delta R = 0.5-4.0$ Å[a]

scatterer	N (±5%)	R (Å)[b]	$\Delta\sigma^2$ (10^{-3} Å^2) (±5%)	ΔE_0 (eV) (±10%)
Pt	2.2	2.67 ± 0.02	4.8	12.0
O*	2.3	2.86 ± 0.08	19.9	1.6
C	2.4	1.92 ± 0.02	2.2	−1.8
O	1.3	2.28 ± 0.02	5.5	−5.8

[a] k^1-variance: absolute part FT, 0.8%; imaginary part FT, 0.3%. [b] Calculated mathematical errors.

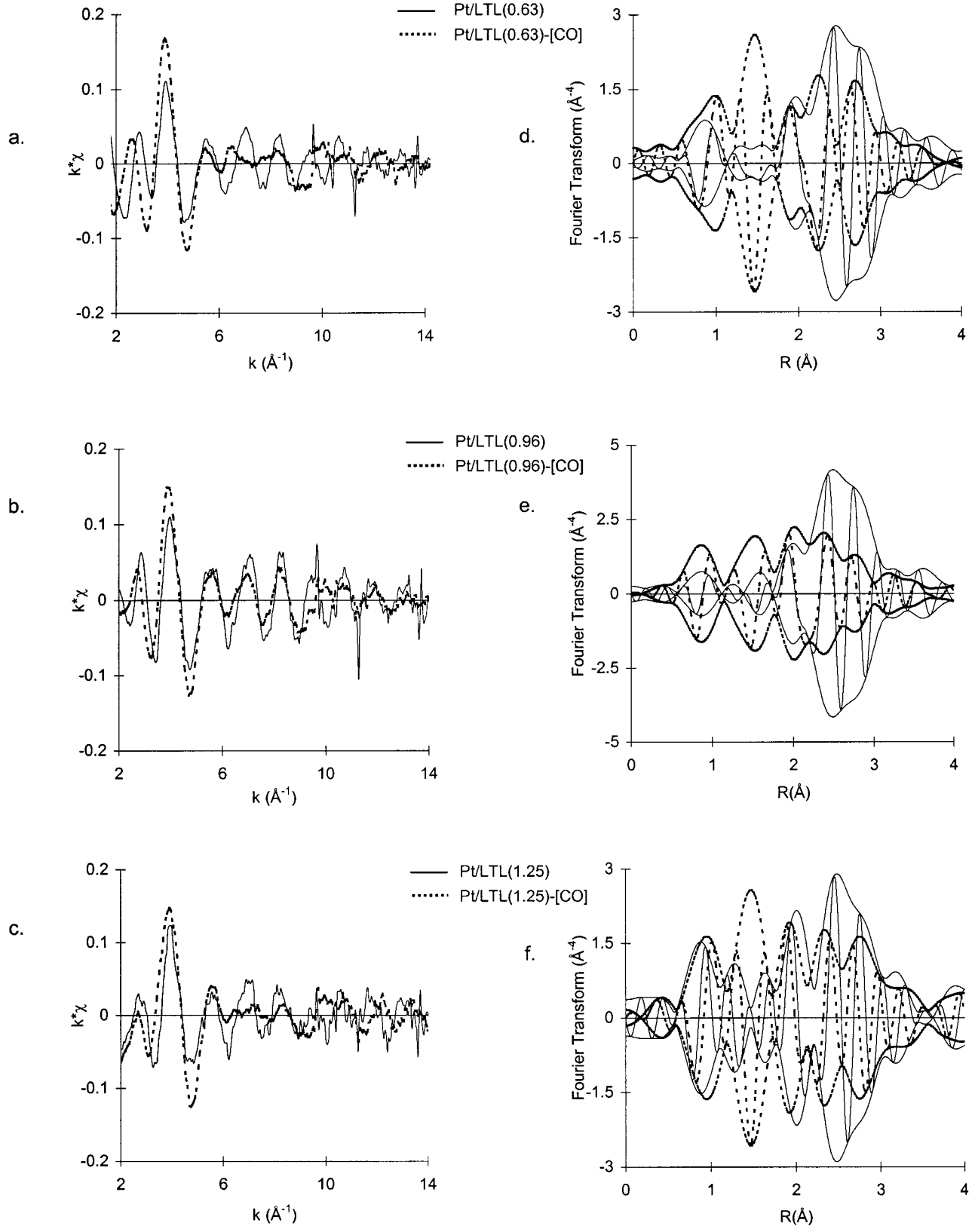

Figure 6. (a)−(c). k^1-weighted experimental data EXAFS data of Pt/LTL (solid line) with (dotted lines): (a) Pt/LTL(0.63)-[CO]; (b) Pt/LTL-(0.96)-[CO]; (c) Pt/LTL(1.25)-[CO]. (d)−(f). Fourier transform (k^3, Δk: 3.0−12.7 Å^{-1}) of spectra in (a)−(c).

inner potential correction (ΔE_0) of the Pt−Pt contribution is quite large compared to reduced Pt/LTL(0.96). This can be due to the difference between the experimental Pt−Pt distance (2.67 Å) and the reference compound (Pt foil, 2.77 Å) or a change in electronic structure of platinum upon adsorption of CO. Further, the Pt−C and Pt−O* contributions show that CO molecules coordinated to Pt are present. The difference in distance of ∼1 Å between C and O* is in good agreement with the intramolecular distance in CO (1.1 Å);[22] however, the error in distance for the Pt−O* contribution is larger than for the other

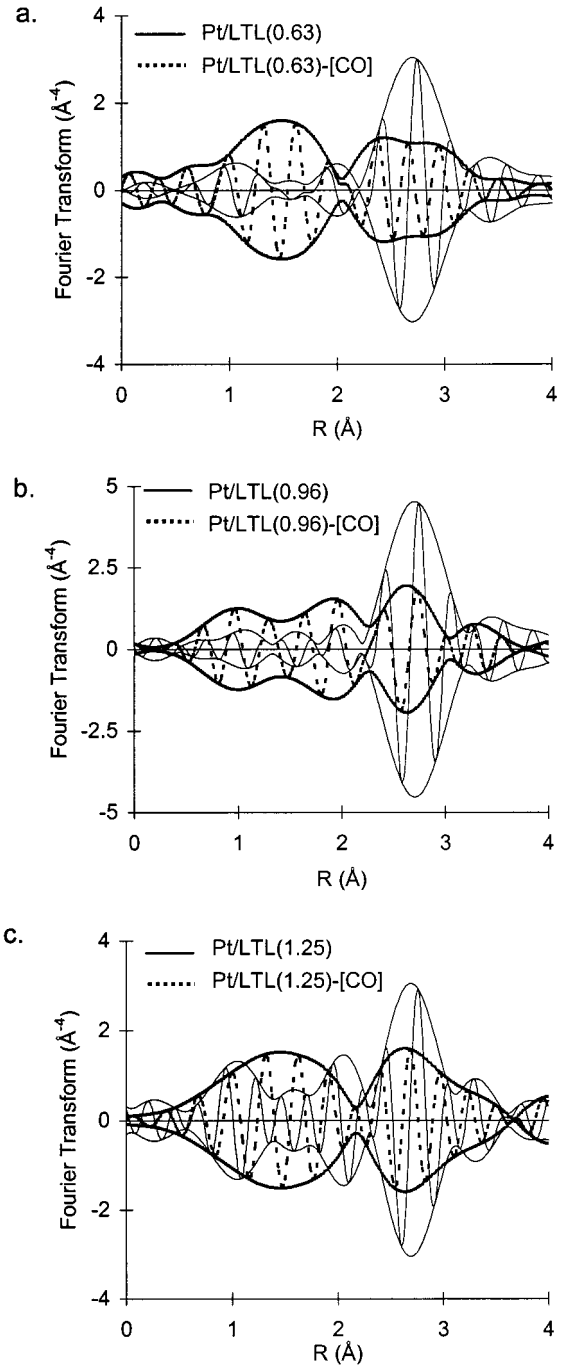

Figure 7. k^3-weighted, Pt−Pt phase corrected Fourier transform (Δk = 6.0−12.7 Å^{-1}) of Pt/LTL (solid line) with (dotted lines): (a) Pt/LTL(0.63)-[CO]; (b) Pt/LTL(0.96)-[CO]; (c) Pt/LTL(1.25)-[CO].

contributions. In addition, the large Debye−Waller factor of 19.9 × 10^{-3} Å^2 indicates a higher disorder in the Pt−O* backscattering function, which may be due to the fact that bound CO on a very small platinum entity can bend freely, creating a larger deviation in the average Pt−O* distance. Moreover, the analysis of the multiple scattering oxygen (O*) contribution is based on a reference made for a linear coordinated CO. Linear coordination will lead to the maximum multiple backscattering amplitude for Pt−O*. As soon as the angle between O*−C−Pt becomes less than 180°, the Pt−O* coordination number and distance as detected with XAFS data analysis will be smaller. The FTIR spectra of Pt/LTL(0.96)-[CO] already showed bridged CO. Since the EXAFS data were calculated assuming only linearly coordinated CO, this results in the higher uncertainty of the Pt−O* distance. Inclusion of both linearly and bridged coordinated CO in the EXAFS analysis was not statistically justified.

The fourth contribution at 2.28 Å in the Fourier transform is most likely due to support oxygen atoms. An attempt to fit this contribution with a Pt−C coordination resulted in a lowered goodness of fit. Furthermore, if there was a Pt−C contribution at 2.28 Å, there also should be a significant Pt−O* contribution at around 3.0−3.4 Å. However, no O* contribution could be detected in the region 3.0−3.4 Å. Recently, based on FTIR experiments, it was suggested that neutral carbonyl complexes were formed from platinum in zeolite LTL upon exposure to CO.[8] The FTIR spectra in that study significantly differed from those of negatively charged Chini complexes.[26] The Pt−Pt coordination number (2.2) and distance (2.67 Å) determined in the present study for Pt/LTL(0.96)-[CO] are similar to those in an anionic Chini complex ($[Pt(\mu CO)(CO)_2]_n^{2-}$) ($N_{Pt-Pt} = 2$, $R = 2.64$ Å).[27] However, the numbers of CO ligands (average of 2.4 for Pt/LTL(0.96)-[CO]) are not alike, since in a Chini complex each Pt atom is surrounded by three carbon atoms (two bridged bound, one linear coordinated). Furthermore, the FTIR spectrum of Pt/LTL(0.96)-[CO] is also different from that of Chini complexes.[26] First, the spectrum of a Chini complex shows a linear and a bridged absorption band with almost the same absorption intensity, while the L/B ratio of Pt/LTL(0.96)-[CO] is much greater than 1. Second, the infrared absorption band of bridged CO in the Chini complex is located at around 1750 cm^{-1}, which is 80 cm^{-1} lower than bridged CO on Pt/LTL-(0.96).

The EXAFS and FTIR data clearly demonstrate that CO adsorption on Pt/LTL(0.96) results in a decrease of the metal particle size, but an aggregate has formed that is different from a Chini complex, as suggested in ref 8. Interestingly, the Pt−$O_{support}$ contribution in the EXAFS data suggests that not only is the three-atom platinum cluster stabilized by CO ligands as in a Chini complex but also the support has an active role in stabilizing the Pt−CO aggregate. To visualize this, Figure 10 depicts a possible structure of Pt/LTL(0.96)-[CO]. The Pt−Pt distance of 2.67 Å and Pt−O distance of 2.28 Å taken into account point to a cluster that fits exactly in the small LTL-pore opening of 7.1 Å. In Figure 10, the coordination of CO to platinum has a L/B ratio of 3, found in the FTIR data, and a Pt−C coordination number of 2, which is close to 2.4 as determined by XAFS spectroscopy. Of course, other geometries of the Pt−CO cluster inside the zeolite pore are possible as well; nevertheless, the good agreement between the size of the Pt−CO aggregate and the zeolite LTL pore and the presence of a significant Pt−$O_{support}$ scattering strongly suggest that the cluster is stabilized by coordination with the zeolite walls.

Comparison of Pt/LTL(0.63)-[CO] and Pt/LTL(1.25)-[CO] with Pt/LTL(0.96)-[CO] in a Pt−Pt emphasized plot (Figure 7) demonstrated that for all catalysts the Pt−Pt contribution decreased after exposure to CO, indicating that the metal particles reconstructed to smaller aggregates for each sample. However, Figures 6 and 7 also show that each sample has a different XAFS spectrum after CO adsorption. Main differences are manifest below 2 Å and above 2.8 Å, where Pt−C and Pt−O* contribute significantly, strongly suggesting that the geometry of the coordination of CO to the metal atoms depends on the zeolite acidity. It was not possible to fully analyze the EXAFS spectra of Pt/LTL(0.63)-[CO] and Pt/LTL(1.25)-[CO] due to the different ratio of linear/bridged CO. It is further not possible to arrive at a unique model describing the EXAFS data,

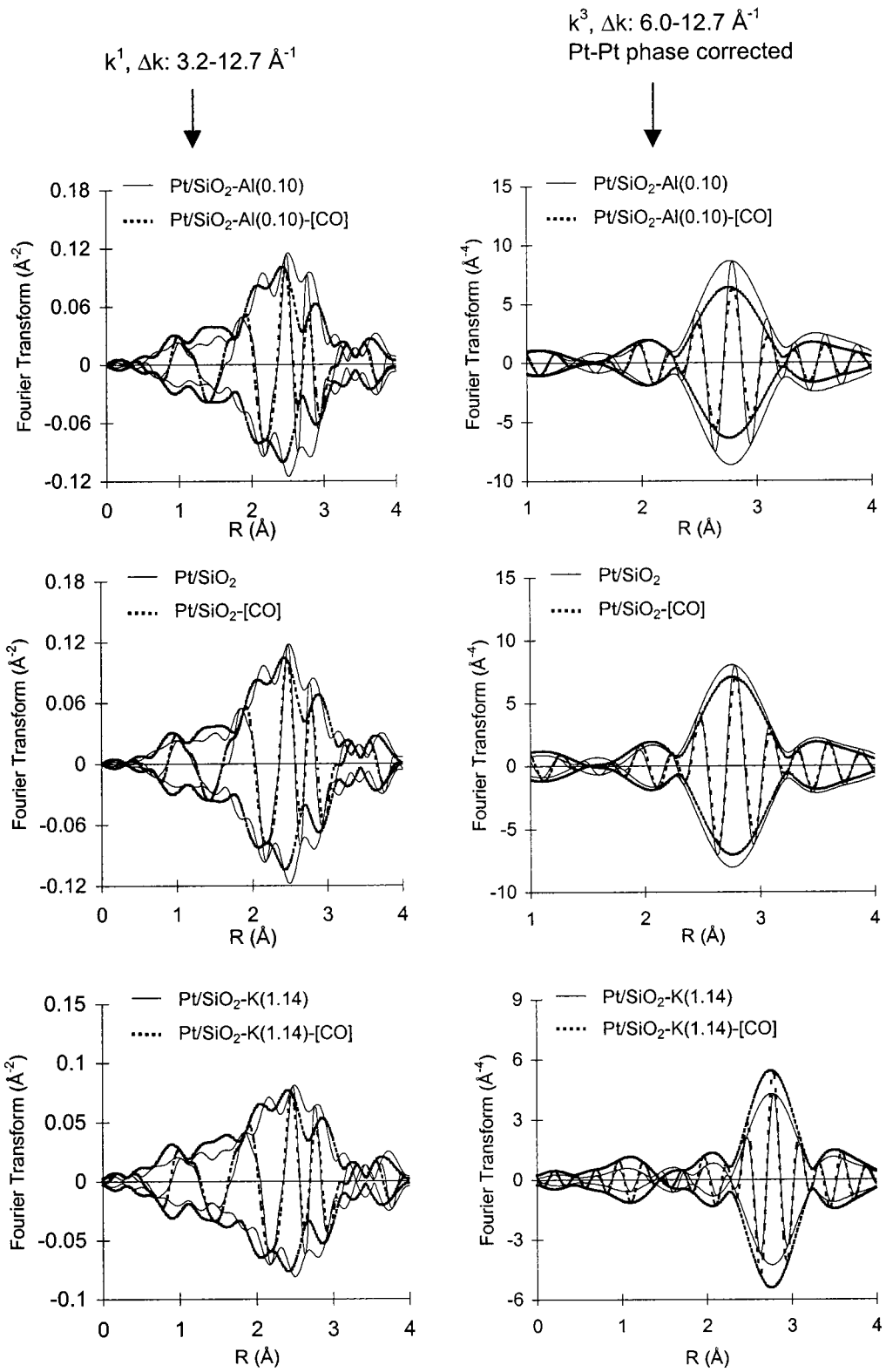

Figure 8. (a)−(c). k^1-weighted Fourier transform (Δk = 3.2−12.7 Å^{-1}) of experimental data EXAFS data of Pt/SiO_2 (solid line) with Pt/SiO_2-[CO] (dotted line): (a) Pt/SiO_2-Al(0.10); (b) Pt/SiO_2; (c) Pt/SiO_2−K(1.14). (d)−(f) k^3-weighted Pt−Pt phase corrected Fourier transform (Δk = 6.0−12.7 Å^{-1}) of same samples.

since (i) the available data range is limiting the number of free parameters and (ii) the Pt−O* contribution is strongly interfering with the Pt−Pt EXAFS. Still, EXAFS showed a change in platinum coordination upon CO adsorption that is different for each support applied. This observation is in line with the FTIR spectra, since these data also showed different sample absorption patterns with changing support acidity.

Influence of CO Adsorption on the Particle Structure of Pt/SiO_2. The platinum particles supported on SiO_2 show much smaller changes upon exposure to CO in comparison with the Pt/LTL samples. The platinum−platinum coordination numbers and distances are only slightly smaller than those of the reduced catalysts measured under hydrogen. In addition to the Pt−Pt contribution, carbon and oxygen scattering (arising from the

TABLE 6: Structural Parameters for Pt/SiO_2-Al(0.10)-[CO], *R*-space Fit, $\Delta k = 3.1-12.8$ Å^{-1}, $\Delta R = 1.0-3.5$ Å[a]

scatterer	N (±5%)	R (Å)[b]	$\Delta\sigma^2$ (10^{-3} Å^2) (±5%)	ΔE_0 (eV) (±10%)
Pt	6.8	2.77 ± 0.03	3.4	2.4
O*	1.1	2.85 ± 0.03	11.4	3.9
C	0.9	1.85 ± 0.02	−0.4	6.7

[a] k^1-variance: absolute part FT, 1.3%; imaginary part FT, 0.4%. [b] Calculated mathematical errors.

TABLE 7: Structural Parameters for Pt/SiO_2-[CO], *R*-Space Fit, $\Delta k = 3.1-12.8$ Å^{-1}, $\Delta R = 1.0-3.5$ Å[a]

scatterer	N (±5%)	R (Å)[b]	$\Delta\sigma^2$ (10^{-3} Å^2) (±5%)	ΔE_0 (eV) (±10%)
Pt	7.3	2.77 ± 0.03	3.1	2.5
O*	1.0	2.84 ± 0.03	10.7	3.6
C	1.0	1.84 ± 0.02	1.0	11.8

[a] k^1-variance: absolute part FT, 1.0%; imaginary part FT, 0.5%. [b] Calculated mathematical errors.

TABLE 8: Structural Parameters for Pt/SiO_2-K(1.14)-[CO], *R*-Space Fit, Δk: $= 3.1-12.8$ Å^{-1}, $\Delta R = 1.0-3.5$ Å[a]

scatterer	N (±5%)	R (Å)[b]	$\Delta\sigma^2$ (10^{-3} Å^2) (±5%)	ΔE_0 (eV) (±10%)
Pt	5.1	2.77 ± 0.03	2.7	1.0
O*	0.8	2.89 ± 0.03	12.5	3.5
C	1.7	1.84 ± 0.02	6.2	15.4

[a] k^1-variance Absolute Part FT: 0.9 %, Imaginary Part FT: 0.5 %. [b] Calculated mathematical errors.

CO molecule) was detected. The Pt−O* contributions had high Debye−Waller factors, similar to those of Pt/LTL(0.96)-[CO]. The distance between carbon and oxygen was also around 1.0 Å, which is in accordance with the intramolecular distance in CO and similar to the C−O distance for Pt/LTL(0.96)-[CO].

The ratio of the Pt−C/Pt−O* coordination numbers steadily increased with rising support alkalinity (Tables 6−8), due to increasing Pt−C coordination number as well as decreasing Pt−O* scattering intensity. Both observations point to increasing amounts of CO in bridged coordination in agreement with the FTIR spectra of these samples. The platinum−support oxygen distance could not reliably be detected in the Pt/SiO_2-[CO] samples, likely due to the Pt−C contribution at 1.84 Å, which is much larger than the Pt−$O_{support}$ contribution.

Consequences for Application of CO−FTIR as a Catalyst Characterization Tool. Several studies have shown differences in the reactivity of small supported metal clusters toward CO. Already in 1978, Primet showed that at liquid nitrogen temperature CO adsorbed onto small supported rhodium particles, while warming to room temperature under CO led to the formation of geminal dicarbonylrhodium species.[28] The structure was later confirmed by EXAFS.[13] It was also shown for rhodium that only very small rhodium metal clusters reconstructed upon CO exposure, while larger clusters were stable.[15] On the other hand, for small palladium particles in zeolite Y, upon adsorption of CO, the metal particles produced a large $Pd_x(CO)_y$ cluster, just fitting inside the supercages.[29] In this study, the platinum particles in zeolite LTL undergo reconstruction and decrease in size when exposed to CO at room temperature. In a different paper we show that this reconstruction of platinum in LTL-(0.96) is temperature dependent.[30] For the larger particles of the Pt/SiO_2 samples, however, little change occurs in the metal particle on CO adsorption. The effect of particle size on the reactivity of the Pt atoms can be understood from the point of view that, in zeolite LTL, particles merely consist of a single

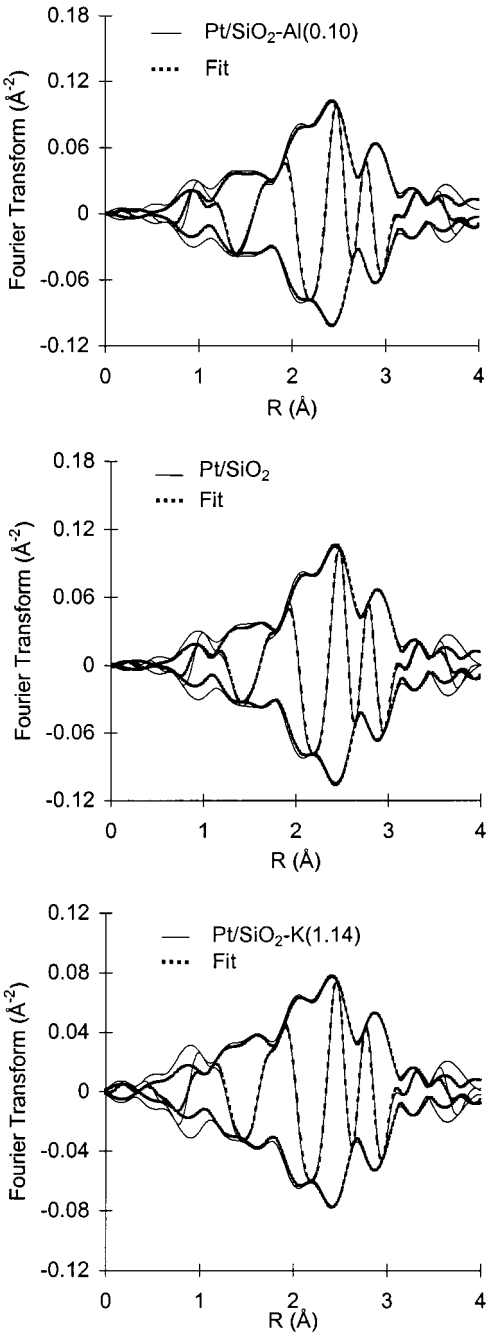

Figure 9. Fourier transform [k^1, $\Delta k = 3.2-12.7$ Å^{-1}] of EXAFS data of Pt/SiO_2-[CO] (solid line) and calculated spectra with parameters given in Tables 6−8 (dashed lines): (a) Pt/SiO_2−Al(0.10)-[CO]; (b) Pt/SiO_2-[CO]; (c) Pt/SiO_2-K(1.14)-[CO].

shell coordination of platinum atoms. Consequently, the Pt atoms have a lower cohesive energy and thus show increased reactivity. In line with this, metal particles supported on silica are much more stable, since they consist of several shells of platinum atoms, which increases the cohesive energy and decreases the reactivity. Recently, a paper was published on DFT calculations and microcalorimetric investigations of CO adsorption on Pt clusters.[31] The authors calculated the heat of formation of neutral Pt−CO clusters from a 10-atom Pt cluster to be only −30 kJ/mol CO, which is only slightly endothermic. The particles in zeolite LTL consist on average of less than 10 atoms; thus the reaction might even be exothermic for these small clusters. In addition, they suggested that the decomposition of Pt particles of 10 atoms could be CO pressure dependent, as was suggested

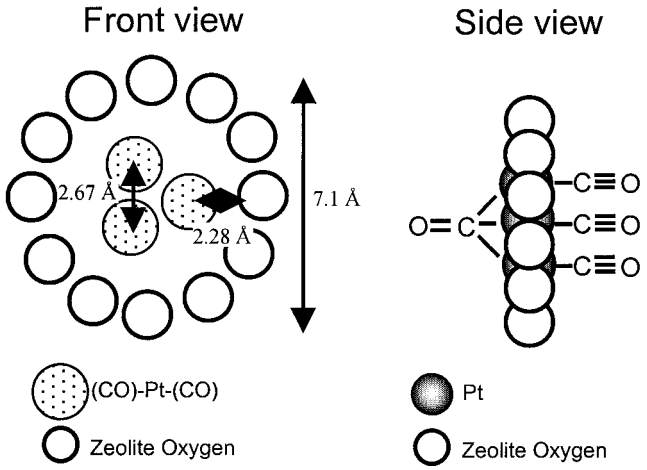

Figure 10. Tentative structure of Pt/LTL(0.96) exposed to CO.

earlier by Stakheev et al.[8] However, since in this study the reactivity toward CO was determined at 1 atm CO pressure for all samples, the stable metal particles on SiO_2 can only be explained by the fact that the particles are larger and consequently more stable.

A particle size dependent reactivity of platinum particles toward CO also explains the slightly decreasing Pt−Pt coordination number (~10%) for the Pt/SiO_2 samples. In addition to the larger average metal particle size, it is likely that there is a particle size distribution. If exclusively very small particles reconstruct upon CO exposure, then only a small fraction of the Pt/SiO_2 particles will be affected, causing a slight decrease in the average Pt−Pt coordination number. An additional aspect of the different behavior of platinum particles on zeolite LTL and SiO_2 could be the stabilizing effect of the support material on the newly formed metal−CO clusters, as was suggested for palladium in zeolite Y.[29]

We have previously shown that there is a decrease in the integrated intensity ratio linear/bridged coordinated CO as well as in the neopentane turnover frequency (TOF) with rising support alkalinity for Pd/LTL, Pt/LTL, and Pt/SiO_2 catalysts.[5,6] The correlation of the linear-to-bridged ratio with TOF was thought to reflect the changes in the electronic structure of the surface platinum atoms in the catalysts. However, the correlation between CO-FTIR and catalysis is not straightforward. The present study demonstrates that the structure of the platinum particles in LTL zeolite probed by FTIR of adsorbed CO are smaller than those of reduced Pt, which are responsible for catalysis. Interestingly, although there has been significant reconstruction, the linear-to-bridged ratio does seem to reflect the changes in electronic properties induced by the support. Recently, this was confirmed by the position of the Pt−H antibonding state relative to the Fermi level as a function of support acidity of the reduced Pt/LTL catalysts.[32]

For Pt/SiO_2 catalysts, CO adsorption has a much smaller effect on the platinum structure due to the larger metal particles. The L/B ratio, in this case, better reflects the changes in electronic properties of the surface metal atoms. As a result, the correlation of L/B ratio with TOF is better for the Pt/SiO_2 catalysts than for Pt/LTL.

Conclusion

Application of CO-FTIR for determination of the electronic structure (reflected in L/B ratio) has to be done with care. Special attention has to be paid with regard to metal particle size. The present study demonstrates that larger platinum particles (i.e., $N_{\text{first shell}} > 5$) on SiO_2 are stable to exposure of CO at room temperature. Smaller particles, supported on zeolite LTL, however, form Pt−CO aggregates after admission of CO.

Although XAFS indicates that CO adsorption results in the formation of smaller metal particles, the correlation with the TOF suggests that the linear-to-bridged ratio is primarily affected by the electronic properties of the Pt particles. In addition, the decrease in L/B ratio with increasing support alkalinity is strong evidence that the support composition induces changes in the electronic properties of the metal particles that, in turn, lead to modification of the catalytic activity.

References and Notes

(1) Kappers, M. J.; Miller, J. T.; Koningsberger, D. C. *J. Phys. Chem.* **1996**, *100*, 3227.

(2) van Hardeveld, R.; Hartog, F. *Adv. Catal.* **1972**, *22*, 75.

(3) Kappers, M. J.; Vaarkamp, M.; Miller, J. T.; Modica, F. S.; van der Maas, J. H.; Koningsberger, D. C. *Catal. Lett.* **1993**, *21*, 235.

(4) Stoop, F.; Toolenaar, F. J. C. M.; Ponec, V. *J. Catal.* **1982**, *73*, 50.

(5) Mojet, B. L.; Kappers, M. J.; Muijsers, J. C.; Niemantsverdriet, J. W.; Miller, J. T.; Modica, F. S.; Koningsberger, D. C. *Stud. Surf. Sci. Catal.* **1994**, *84*, 909.

(6) Mojet, B. L.; Kappers, M. J.; Miller, J. T.; Koningsberger, D. C. *Stud. Surf. Sci. Catal.* **1996**, *101*, 1165.

(7) van Santen, R. A. *J. Chem. Soc., Faraday Trans. 1* **1987**, *8*, 1915.

(8) Stakheev, A. Yu.; Shpiro, E. S.; Jaeger, N. I.; Schulz-Ekloff, G. *Catal. Lett.* **1995**, *34*, 293.

(9) de Mallmann, A.; Barthomeuf, D. *Catal. Lett.* **1990**, *5*, 293.

(10) Bischoff, H.; Jaeger, N. I.; Schulz-Ekloff, G.; Kubelkove, L. *J. Mol. Catal.* **1993**, *80*, 95.

(11) Chang, J.-R.; Xu, Z.; Purnell, S. K.; Gates, B. C. *J. Mol. Catal.* **1993**, *80*, 49.

(12) Li, G.-J.; Fujimoto, T.; Fukuoka, A.; Ichikawa, M. *Catal. Lett.* **1992**, *12*, 171.

(13) van't Blik, H. F. J.; van Zon, J. B. A. D.; Huizinga, T.; Vis, J. C.; Koningsberger, D. C.; Prins, R. *J. Phys. Chem.* **1983**, *87*, 2264.

(14) Koningsberger, D. C.; van 't Blik, H. F. J.; van Zon, J. B. A. D.; Prins, R. *Proc. Int. Congr. Catal., 8th* **1984**, *5*, 120.

(15) van't Blik, H. F. J.; van Zon, J. B. A. D.; Koningsberger, D. C.; Prins, R. *J. Mol. Catal.* **1984**, *25*, 379.

(16) de Mallmann, A.; Barthomeuf, D. *Stud. Surf. Sci. Catal.* **1989**, *46*, 429.

(17) Vaarkamp, M.; Mojet, B. L.; Kappers, M. J.; Miller, J. T.; Koningsberger, D. C. *J. Phys. Chem.* **1995**, *99*, 16067.

(18) Hayes, T. M.; Boyce, J. B. *Solid State Phys.* **1982**, *237*, 283.

(19) Duivenvoorden, F. B. M.; Koningsberger, D. C.; Uh, Y. S.; Gates, B. C. *J. Am. Chem. Soc.* **1986**, *108*, 6254.

(20) Koningsberger, D. C. In *Neutron and Synchrotron Radiation for Condensed Matter Studies, Vol. II, Applications to Solid State Physics and Chemistry*; Baruchel, J., Hodeau, J. L., Lehmann, M. S., Regnard, J. R., Schlenker, C., Eds.; Springer-Verlag: Berlin, 1994; pp 213−244.

(21) Kampers, F. W. H.; Engelen, C. W. R.; van Hooff, J. H. C.; Koningsberger, D. C. *J. Phys. Chem.* **1990**, *94*, 8574.

(22) van Zon, F. B. M.; Maloney, S. D.; Gates, B. C.; Koningsberger, D. C. *J. Am. Chem. Soc.* **1993**, *115*, 10317.

(23) Vaarkamp, M.; Modica, F. S.; Miller, J. T.; Koningsberger, D. C. *J. Catal.* **1993**, *144*, 611.

(24) Koningsberger, D. C.; Vaarkamp, M.; Muñoz Paez, A.; van Zon, F. B. M. Iwasawa, Y., Ed.; In *X-ray absorption fine structure for catalysts and surfaces*; World Scientific: London, 1996; Vol. 2, pp 257−272.

(25) Vaarkamp, M.; Miller, J. T.; Modica, F. S.; Koningsberger, D. C. *J. Catal.* **1996**, *163*, 294.

(26) Schulz-Ekloff, G.; Lipski, R. J.; Jaeger, N. I.; Hulstede, P. *Catal. Lett.* **1995**, *30*, 65.

(27) Li, G. J.; Fujimoto, T.; Fukuoka, A.; Ichikawa, M. *J. Chem. Soc., Chem. Commun.* **1991**, 1337.

(28) Primet, M. *J. Chem. Soc., Faraday Trans. 1* **1978**, *74*, 2570.

(29) Sheu, L. L.; Knozinger, H.; Sachtler, W. M. H. *J. Am. Chem. Soc.* **1989**, *111*, 8125.

(30) Mojet, B. L.; de Vooys, A. C. A.; Koningsberger, D. C. Manuscript in preparation.

(31) Watwe, R. M.; Spiewak, B. E.; Cortright, R. D.; Dumesic, J. A. *Catal. Lett.* **1998**, *51*, 139

(32) Ramaker, D. E.; Mojet, B. L.; Garriga-Oostenbrink, M. T.; Miller, J. T.; Koningsberger, D. C. *Phys. Chem. Chem. Phys.*, submitted.